Document Version:

This is the Published Version.

Enquiries

If you believe this document infringes copyright, please contact Research & Scholarly Communications at rsc@herts.ac.uk

The rotation of the halo of NGC 6822 from the radial velocities of carbon stars

Graham P. Thompson,[★] Sean G. Ryan and Lisette F. Sibbons

School of Physics, Astronomy and Mathematics, University of Hertfordshire, College Lane, Hatfield AL10 9AB, UK

ABSTRACT

Using spectra taken with the AAOmega spectrograph, we measure the radial velocities of over 100 stars, many of which are intermediate age carbon stars, in the direction of the dwarf irregular galaxy NGC 6822. Kinematic analysis suggests that the carbon stars in the sample are associated with NGC 6822, and estimates of its radial velocity and galactic rotation are made from a star-by-star analysis of its carbon star population. We calculate a heliocentric radial velocity for NGC 6822 of $-51 \pm 3 \, \mathrm{km \, s^{-1}}$ and show that the population rotates with a mean rotation speed of $11.2 \pm 2.1 \, \mathrm{km \, s^{-1}}$ at a mean distance of 1.1 kpc from the galactic centre, about a rotation axis with a position angle of $26° \pm 13°$, as projected on the sky. This is close to the rotation axis of the H I gas disc and suggests that NGC 6822 is not a polar ring galaxy, but is dynamically closer to a late-type galaxy. However, the rotation axis is not aligned with the minor axis of the AGB isodensity profiles and this remains a mystery.

Key words: techniques: radial velocities – stars: AGB and post-AGB – galaxies: individual: NGC 6822 – galaxies: kinematics and dynamics – Local Group – infrared: stars.

1 INTRODUCTION

NGC 6822 (Barnard's galaxy) is a relatively bright and well-studied dwarf irregular galaxy. It lies within the Local Group (LG), quite close to the Milky Way, and is the third nearest dwarf irregular galaxy after the Large and Small Magellanic Clouds. It was the first object to be shown to lie outside the Milky Way by Edwin Hubble (Hubble 1925). It has no known close companions and lies in a region relatively devoid of other galaxies (de Blok & Walter 2000). Despite its apparent isolation, there is some evidence of tidal interaction and a burst of star formation 100–200 Myr ago (de Blok & Walter 2000 and references therein).

The location of NGC 6822 has a range of published values for right ascension (α) and declination (δ),[1] but for the purposes of this paper we use $\alpha = 19^h 44^m 56^s$, $\delta = -14° 48' 06''$ (J2000). This is at the centre of a 3 deg^2 field used by Sibbons et al. (2012, 2015) and is adopted here for consistency, since this study uses spectra drawn from their sample.

The galactic distance is variously reported to lie between 450 to over 500 kpc. For the purposes of this paper, its distance is not important, but where we do use it, we again adopt the same value as Sibbons et al. (2012, 2015), 490 ± 40 kpc, for consistency with that work. This is the value quoted in Mateo (1998). Sibbons et al. (2012, 2015) also quotes a distance modulus for NGC 6822 of

$(m - M)_0 = 23.45 \pm 0.15 \, (\approx 490 \pm 34 \, \mathrm{kpc})$. In recent years, papers have been published which have provided new distance moduli using Cepheid variables. Many of these re-estimates have reduced the radial distance to NGC 6822 by about 10 per cent from the value used herein. The distance modulus derived by Gieren et al. (2006) is $(m - M)_0 = 23.312 \pm 0.021 \, (\approx 460 \pm 4.4 \, \mathrm{kpc})$, Feast et al. (2012) gives $(m - M)_0 = 23.40 \pm 0.05^2 \, (\approx 479 \pm 11 \, \mathrm{kpc})$, and Rich et al. (2014) gives $(m - M)_0 = 23.38 \pm 0.02_{\mathrm{stat}} \pm 0.04_{\mathrm{sys}}$ ($\approx 474 \pm 13_{\mathrm{tot}}$ kpc). In Whitelock et al. (2013), an alternative to Cepheid variables is proposed using Mira variables for distance measurement. These are AGBs which vary in magnitude over periods of several hundred days. NGC 6822 is used as one example of the measurement of distance using Mira variables and after calibration of the method using Miras in the Large Magellanic Cloud, the distance module for NGC 6822 is given as $(m - M)_0 = 23.56 \pm 0.03 \, \mathrm{mag} \, (\approx 515 \pm 7 \, \mathrm{kpc})$, somewhat greater than the other estimates.

Morphologically, NGC 6822 has three components: a gaseous H I disc (de Blok & Walter 2000), an outer spheroid of stars containing red giant branch (RGB) and asymptotic giant branch (AGB) stars (Letarte et al. 2002; Battinelli, Demers & Kunkel 2006; Demers, Battinelli & Kunkel 2006; Sibbons et al. 2012, 2015) and a small central core of young stars (Hodge et al. 1991). The H I gas disc appears to lie at a position angle (PA) of $\sim 130°$ when observed from tip to tip (see fig. 1 of de Blok & Walter 2000), but it also appears

---

[★] E-mail: g.p.thompson@herts.ac.uk

[1] SIMBAD: $\alpha = 19^h 44^m 56^s.199$, $\delta = -14° 47' 51''.29$ (J2000). NED: $\alpha = 19^h 44^m 57^s.7$, $\delta = -14° 48' 12''$ (J2000). McConnachie (2012): $\alpha = 19^h 44^m 56^s.6$, $\delta = -14° 47' 21''$ (J2000).

[2] Feast et al. (2012) does not claim any precision with the error value, owing to the difficulty in measuring the true uncertainty in the value of the distance modulus.

to twist. In Weldrake, de Blok & Walter (2003), the PA is stated as ∼110°, close to the major axis of the central body of the disc as projected on the sky. Letarte et al. (2002) shows that carbon stars lie well outside the H I disc and Demers et al. (2006) and Battinelli et al. (2006) show that the isophotes of RGBs of NGC 6822 are also elliptical, where the major axis PA changes from ∼65° for the outermost contour to ∼80° for the innermost contour (see fig. 1 of Demers et al. 2006).

Much of the published velocity data for NGC 6822 have been derived from the H I gas content of NGC 6822 using the 21 cm line (Weldrake et al. 2003; Koribalski et al. 2004). Koribalski et al. (2004) measure a heliocentric radial velocity, V_{helio}, of -57 ± 2 km s^{-1} for NGC 6822 from its HIPASS spectrum, and this now a commonly cited value. Mateo (1998), and sources therein, also provide V_{helio} based on the H I component, $V_{\odot, \mathrm{radio}}$ of -54 ± 6 km s^{-1}, and Weldrake et al. (2003) similarly provides an H I derived systemic (radial) velocity[3] in the range -53.3 km s^{-1} to -54.7 km s^{-1} at the centre of the H I gas.

Rotation of the gas disc has also been measured at 21 cm. Mateo (1998) provides a value for the rotation of the H I disc, $v_{\mathrm{rot, ISM}}$, of 47 ± 3 km s^{-1}, and Weldrake et al. (2003) show that the velocity of the H I disc ranges from -100 km s^{-1} at the NW extreme (blueshifted) to $+10$ km s^{-1} at the SE extreme (redshifted). McConnachie (2012) quotes a peak observed rotation speed of 47 ± 2.0 km s^{-1}, uncorrected for inclination or asymmetric drift, citing Koribalski et al. (2004) and Weldrake et al. (2003).

With regard to the stellar kinematics of NGC 6822, Mateo (1998), and references therein, provide a value of V_{helio} based on optical measurements of $V_{\odot, \mathrm{opt}} = -53 \pm 4$ km s^{-1}. Kirby et al. (2014) studies the kinematics of seven isolated dwarf galaxies in the LG from the radial velocities of red giant stars, including NGC 6822, and derives a mean heliocentric radial velocity, $\langle V_{\mathrm{helio}} \rangle$, of -54.5 ± 1.7 km s^{-1} for NGC 6822.

However, while there are published data for V_{helio}, there are little regarding stellar rotation. Many publications refer to Demers et al. (2006) for stellar rotation, where the radial velocities for 110 carbon stars lying within 15 arcmin (∼2.1 kpc) of the H I major axis, taken from a sample in Letarte et al. (2002), are measured, although the individual stellar measurements are not published. A variation in residual velocity along the major axis of the outermost RGB isophote is interpreted to be a signature of rotation about the minor axis. As a result, the paper suggests that the carbon stars appear to rotate about an axis roughly perpendicular to the rotation axis of the H I disc, resembling a polar ring galaxy (PRG). It would be extraordinarily useful if NGC 6822 is a PRG, since they are very rare. The Sloan Polar-Ring Catalogue, which uses images from the Sloan Digital Sky Survey, includes only six confirmed PRGs from a total of just 275 candidates. Discovery of a nearby PRG would present a remarkable opportunity to study these galactic types at close hand. In a separate publication (Demers & Battinelli 2007) suggest that radial velocities of individual NGC 6822 giants might give some insight into rotation of the stellar population.

Kirby et al. (2014) checked for signs of rotation in their sample of seven dwarf galaxies, and found that only the Pegasus dwarf irregular showed obvious signs. For NGC 6822, they refer to the findings of Demers et al. (2006). They comment that while a rotation of the order of ∼10 km s^{-1} is possible in NGC 6822, their data were too highly obscured by velocity dispersions to be certain.

The published studies of the galaxy's stellar rotation are complemented by other studies of the motion of globular clusters (Veljanoski et al. 2015) and planetary nebulae (PNe; Flores-Durán et al. 2014). Veljanoski et al. (2015) studies the globular cluster (GC) system of NGC 6822, in which eight GCs are presently identified (see Table 1 therein). The radial velocities of six of the GCs are given and $\langle V_{\mathrm{helio}} \rangle$ is deduced to be between -59 and -60 km s^{-1}. The spatial distribution of the GCs in their data is rather linear and lies approximately parallel to the major axis of the AGB isophotes. Three possible dynamical models are considered.

(i) 'Disc model', in which the rotation axes are similar to that suggested by Demers et al. (2006). The resulting rotation rate is 12 ± 10 km s^{-1}.

(ii) 'Cigar model', where the cluster system shares the same rotation axis as the H I disc. In this case the rotation rate is determined to be 56 ± 31 km s^{-1}.

(iii) A scenario where there is no net rotation by disconnecting any relationship between the gas disc and the stellar component.

In none of these models are they able to independently determine the PA of the rotation axis owing to the small number of objects in their sample of GCs, but their preferred case is the 'Disc model', owing to its low rotation rate. They argue that in the case of the 'Cigar model' the rotation is too high, and would cause the sample to flatten into a disc which they do not observe.

In Flores-Durán et al. (2014), the motion of 10 PNe in the galaxy are studied. PNe are the evolutionary stage reached by AGBs after the end of their lives, and may thus provide complementary kinematic information of the galaxy. Flores-Durán et al. (2014) compute the mean $\langle V_{\mathrm{helio}} \rangle$ of the PNe to be -57.8 km s^{-1}. They compare their result with four extended star clusters (ESGs) which have a mean V_{helio} of -88.3 km s^{-1} (Hwang et al. 2014) and with a C-star mean V_{helio} of -32.9 km s^{-1} derived by Hwang et al. (2014). The ESGs lie ∼10.5 kpc from the centre of NGC 6822 and show no signs of rotation (Hwang et al. 2014). Flores-Durán et al. (2014) infer that the PNe, C-stars and clusters belong to different dynamical systems, but with so few PNe, they are unable to reliably fit the radial velocity data to either system.

This paper provides the results of a new study of the kinematics of NGC 6822, based on the spectra of individual stars obtained in 2011 by Sibbons et al. (2015), and follows studies by Sibbons et al. (2012, 2015) which classify stars, photometrically and spectroscopically, from a set taken from the catalogue of Letarte et al. (2002). These studies were able to distinguish C-type and M-type AGBs from other types, so that although Demers & Battinelli (2007) cautions that the separation of carbon stars associated with NGC 6822 from foreground Galactic dwarfs might be difficult, our present study has the advantage of using the spectra of stars which have already been classified as carbon stars in NGC 6822, with a high degree of confidence.

The radial velocities of well over 100 stars within a 4 kpc radius of the centre of NGC 6822, (the *inner region*), and well over 100 stars outside the 4 kpc radius, (the *outer region*), are measured and reported. In the inner region many of these stars are classified as carbon stars and are expected to be associated with the galaxy (Sibbons et al. 2015). In the outer region, most of the stars are expected to be foreground Milky Way stars (Sibbons et al. 2012, 2015).

Based on the aggregated sample of carbon stars in the inner region, a value for the heliocentric radial velocity of NGC 6822 is derived. The kinematics of individual stars in the sample indicate that they belong to the same population, supporting Sibbons et al. (2015). Moreover, the radial velocity measurements are accurate

---

[3] We assume all velocities quoted in Weldrake et al. (2003) are corrected to heliocentric.

Table 1. The first 18 lines of the individual results for objects meeting the criteria ($hght \geq 0.2$, -200 km s^{-1} $\leq V_{\rm helio} \leq +200$ km s^{-1}). The full table can be found in Appendix A to the electronic version of this paper. Columns 1 and 2: fibre number and the target identifier, respectively, as defined by Sibbons et al. (2015). Columns 3 and 4: right ascension (RA) and declination (Dec) of each object (J2000) according to Sibbons et al. (2015). Column 5: *I*-band magnitude of C-type AGBs in the inner region from the catalogue of Letarte et al. (2002). Column 6: distance of the object from the putative galactic centre ($\alpha = 19^{\rm h}44^{\rm m}56^{\rm s}$ (296°2333), J2000 and $\delta = -14°48'06''$ ($-14°8017$), J2000 centred on the optical co-ordinates of NGC 6822 adopted by Sibbons et al. (2012, 2015) and a galactic distance of 490 kpc (Mateo 1998). Columns 7 and 8: photometric classification of each object from Sibbons et al. (2012), and its corresponding spectroscopic classification from Sibbons et al. (2015). Columns 9 and 13: SNR of each object calculated in the band 8560–8650 Å for the nights of 2011 August 30 and 2011 August 31, respectively. Columns 10, 11 and 12: *hght*, the heliocentric radial velocity ($V_{\rm helio}$) and the velocity error ($V_{\rm err}$) returned from *fxcor* for the night of 2011 August 30. Columns 14, 15 and 16: *hght*, the heliocentric radial velocity ($V_{\rm helio}$) and the velocity error ($V_{\rm err}$) returned from *fxcor* for the night of 2011 August 31. Column 17: flag showing which objects were used in the composite templates: 'C' for the C-type composite and 'M' for the M-type composite.

										Objects meeting the criteria ($hght \geq 0.2$, -200 km s^{-1} $\leq V_{\rm helio} \leq +200$ km s^{-1})						
(1)	(2)	(3)	(4)	(5)	(6)	(7)	(8)	(9)	(10)	(11)	(12)	(13)	(14)	(15)	(16)	(17)
										2011 August 30				2011 August 31		
#Fibre	ID	RA (°)	Dec (°)	*I* band (mag)	distance^a (kpc)	phot. class.	spec. class.	SNR	*hght*	$V_{\rm helio}$ (km s^{-1})	$V_{\rm err}$ (km s^{-1})	SNR	*hght*	$V_{\rm helio}$ (km s^{-1})	$V_{\rm err}$ (km s^{-1})	Flag
1	217716	296.23	−14.86	19.3	0.52	M	Ce:	7	0.39	−10	49	9	0.48	−35	36	C
2	239630	296.33	−14.95	19.4	1.52	C*	C:	6	0.43	−55	41	7	0.54	−55	27	C
3	210316	296.43	−14.83	18.9	1.69	M	C:	5	0.59	15	25	6	0.76	−11	16	C
4	174035	296.37	−14.71	19.1	1.4	M*	C	3	0.37	−26	57	5	0.27	−43	67	C
6	199974	296.37	−14.8	19.2	1.17	M	C	−	−	−	−	9	0.65	4	24	C
7	194949	296.35	−14.78	18.9	1	C*	C:	12	0.72	−1	34	18	0.75	−14	23	C
8	242030	296.35	−14.96	18.8	1.64	−	−	6	0.6	−53	21	9	0.7	−62	22	−
9	220271	296.39	−14.87	−	1.43	−	−	5	0.48	−28	40	8	0.59	−63	27	−
10	188246	296.49	−14.76	18.3	2.12	M	C:	6	0.57	−40	29	10	0.8	−39	16	C
11	172656	296.54	−14.71	19.3	2.66	C*	C	5	0.29	−125	69	8	0.39	−70	41	C
12	211898	296.31	−14.84	18.8	0.7	M	C	9	0.57	−31	26	7	0.74	−21	20	C
14	246838	296.54	−14.98	−	2.99	−	−	4	0.36	−78	37	5	0.57	−61	28	−
15	206867	296.3	−14.82	−	0.59	−	−	7	0.42	1	58	8	0.42	−3	38	−
17	225812	296.32	−14.9	−	1.06	−	−	4	0.33	0	75	6	0.51	−10	31	−
18	190283	296.34	−14.76	19.6	0.96	M	C	6	0.45	−44	33	5	0.36	−51	36	C
19	168284	296.41	−14.69	19.0	1.78	C*	C:	9	0.48	40	42	10	0.48	21	34	C
21	213379	296.24	−14.85	19.9	0.39	C*	Ce:	4	0.4	−25	42	−	−	−	−	C
22	200573	296.27	−14.8	19.0	0.34	M	Ce	8	0.37	10	73	9	0.72	−12	17	C

^{a}Different catalogues and data bases have differing values for the centroid of NGC 6822. These values are adopted to be consistent with Sibbons 2012, Sibbons 2015.

enough to reveal rotation of the stellar component about an axis through the centre of the galaxy, and to derive its rotational speed and a new PA for the axis of rotation. In Section 2, we discuss the data set, its origins and its limitations. In Section 3, we discuss the method used to analyse the data set including the selection of objects for analysis. In Section 4, we discuss the results and in Section 5, we draw conclusions.

2 OBSERVATIONS AND DATA

This study uses AGB stars as tracers of kinematic properties of the galaxy. AGB stars are amongst the brightest stars in an intermediate-age or old stellar population and can be resolved in galaxies beyond the Milky Way, making it possible to study them individually. AGBs tend to divide into those with oxygen-rich atmospheres (M-types), and those with carbon-rich atmospheres (C-types or carbon stars). They have relatively low surface temperatures, $T_{\rm eff}$, ranging from as low as 2200 K (Matthews, Gérard & Le Bertre 2015) for old stars near the end of their lives up to $\sim$4000 K for intermediate age stars.[4] The continuum peaks at wavelengths in the near-infrared, with increasing brightness through the *I, J, H* and *K* bands.

The spectrum of a typical AGB contains a number of absorption features, predominantly broad TiO bands in M-type AGBs, broad CN bands in C-type AGBs. The *I*-band spectral region also contains the Ca II triplet lines in both types of AGB. The Ca II triplet lines are ideal for measuring radial velocities as they are narrow atomic features and lie in a position where the continuum is relatively strong. In this study, we use the spectra of carbon-rich AGBs classified by Sibbons et al. (2015) as follows: confirmed C-type stars (C); tentative C-type stars (C:), confirmed C-type stars which exhibit H α and sometimes [S II] and [N II] emission (Ce) and tentative C-type stars which similarly exhibit emission (Ce:).

Wide band, low-resolution spectra for 323 target objects, out to $\approx$8 kpc from the galactic centre, were obtained using the AAOmega multifibre spectrograph on 2011 August 30 and 31 (Sibbons et al. 2015). An optical fibre was placed over each target object position on the field plate of the spectrograph and throughout this paper, objects are referred to by their fibre number. Wide band gratings 385R and 580V were used in the spectroscopy but this study uses only the spectra from grating 385R, which has a bandpass from 5687 to 8856 Å, covering the Ca II triplet, dispersed at 1.6 Å pixel^{-1}. The spectra were reduced to science frames, using the AAOmega pipeline. The spatial position of each object is plotted in Fig. 1, which shows 135 objects in the inner region, and 188 objects in the outer region. 98 black points and one red point show the positions of the C-type AGBs. The red point is the location of object #31 which was utilized in the processing of the data described later. Three
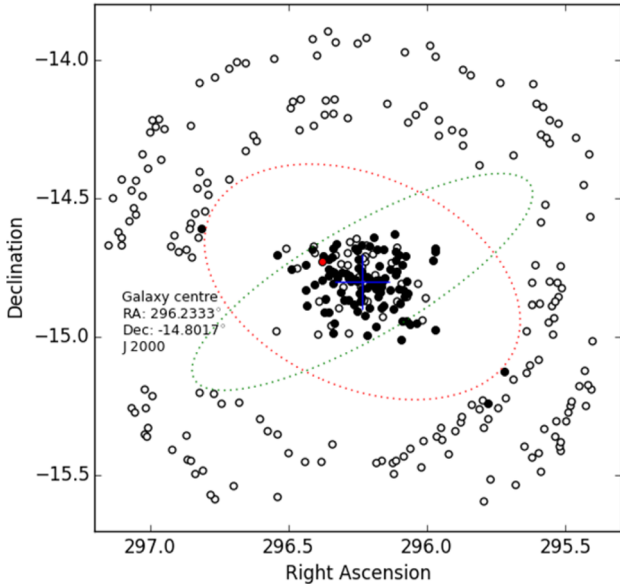
---

[4] In van Belle et al. (2013), 12 carbon stars are found to be in a range of $T_{\rm eff} = 2381 \pm 81$–$3884 \pm 161$ K, with a mean at 2800 ± 270 K.

Figure 1. The locations of 323 NGC 6822 objects targeted by Sibbons et al. (2015), shown over 1°.8 of the sky. The black points and red point show 99 objects classified by Sibbons et al. (2015) as C-type AGBs. The red point marks object #31, which is discussed in the text. The three outermost C-type AGBs lie more than 4 kpc from the galactic centre and were not used in the analysis. The open circles mark the remaining objects which are given other classifications. The dotted ellipses approximate the location and extent of the gas disc (de Blok & Walter 2000) and the outermost stellar isodensity profile (Demers et al. 2006). The concentric appearance of the outer objects is due to the layout of the fibres on the spectrograph field plate.

black points located just outside the outermost isodensity profile were not used in the analysis, so the total number of carbon stars used is 96. Ellipses which reproduce the location and extent of the gas disc and outermost RGB isodensity profile of NGC 6822 are also plotted in Fig. 1.

Fig. 2 shows the spectra of a typical C-type AGB, object #31, for both observing nights. It is evident that the spectrum of August 31 has a higher count in the continuum than that of August 30 and this results in a correspondingly higher signal-to-noise ratio, SNR. This is generally the case for all spectra and led us to place more weight on the results for the night of August 31. The waveband containing the Ca II triplet is shaded in grey in the left-hand panel and its absorption features indicated at 8498.02, 8542.09, and 8662.14 Å (rest) in the right-hand panel.

Although the velocity resolution of the grating was rather low, $\approx$56 km s^{-1} pixel^{-1} in the Ca II triplet waveband of interest, and the individual errors rather higher, there were enough stars present in the sample to reduce the standard error in the mean velocity to $\sim$8 per cent.

3 RADIAL VELOCITY MEASUREMENTS

To measure relative velocities, we used the cross-correlation technique of Tonry & Davis (1979), as implemented in the IRAF[5] routine *fxcor*, star by star. We produced two composite spectra from the

[5] IRAF is distributed by the National Optical Astronomy Observatory, which is operated by the Association of Universities for Research in Astronomy (AURA) under a cooperative agreement with the National Science Foundation.

spectra of the AGBs in the sample, which were used as the template required by this technique. One template was made from C-type AGBs from the inner region, and the second from the dM-type stars in the outer region as classified by Sibbons et al. (2015). Both templates were corrected to the 'rest frame', and then used to measure the radial velocities of the stars. The C-type template was used for all stars, while the M-type template was used for the objects in the outer region only.

The use of a composite template ensures that its spectrum is well matched to the object spectra, that is, it includes the same instrument and observing systematics as the object spectra. Moreover, the combination process makes a significant reduction in the noise content in the template, an important consideration as our spectra had originally been taken with a relatively short exposure time. The composite template spectra are shown in Fig. 3. The undulations in the C-type spectrum are due to the remaining Ca II triplet and to CN absorption lines.

fxcor generates a cross-correlation function of an object spectrum and the template spectrum, and fits a Gaussian to it. As the template is in the rest frame, the position of the Gaussian peak with respect to the baseline determines the radial velocity, V_r, of the object, and application of the heliocentric correction[6] yields an object's heliocentric radial velocity, V_{helio}. Initial experimentation and visual inspection were performed to find the best parameters to use in *fxcor* to minimize errors and maximize the number of successful cross-correlation operations. It was found that a 9 pixel Gaussian fit ($\equiv$13.5 Å or 717 km s^{-1}) fitted the shape of the peak of the cross-correlation function closely and did not limit the number of successful cross-correlations. All spectra were truncated to the waveband 8440–8710 Å, which covers the Ca II triplet, to ensure that IRAF calculated the velocity resolution appropriate to this waveband, and the cross-correlation bandwidth was restricted to 8450–8700 Å to reduce spectral noise coming from outside this waveband.

The quality of the spectra is important. As well as low spectral resolution, many of our spectra had low SNR ($<$10 pixel^{-1}), causing noisy cross-correlation functions. These sometimes returned unreliable results or failed to give a result at all. To overcome these difficulties, selection criteria were adopted to rule out any spectra which might give rise to unreliable results. The criteria were based on the strength of the cross-correlation function, *hght* and on the radial velocities returned by *fxcor* as described below.

It was found, by inspection, that cross-correlation functions with *hght* $>$0.4 give a strong peak with low sidebands, but those with *hght* $<$0.2 do not. In these cases, the peaks are weak with respect to the sidebands and in some cases, multiple peaks occur. Between these limits, the quality of the cross-correlations degrades but useful results can be achieved in many cases. After visual inspection of each cross-correlation function, we excluded all cross-correlation functions where *hght* $<$0.2.

We then examined the *fxcor* velocity returns. In a number of cases, unrealistically high values of V_{helio} were observed. These can come about by selection of the 'wrong' peak by *fxcor* in noisy or multipeak cross-correlation functions. Values of V_{helio} as large as $\pm$1554, $\pm$4184 or $\pm$5734 km s^{-1} arise, which are regarded as unrealistic, and such values tend to be associated with *hght* values close to or less than 0.2. The distribution of velocities returned from *fxcor*, corrected to V_{helio}, was analysed and showed that most velocities fall within $\pm$200 km s^{-1}. All cross-correlation functions where

[6] -19.5 km s^{-1} (2011 August 30) and -19.8 km s^{-1} (31 August 2011).
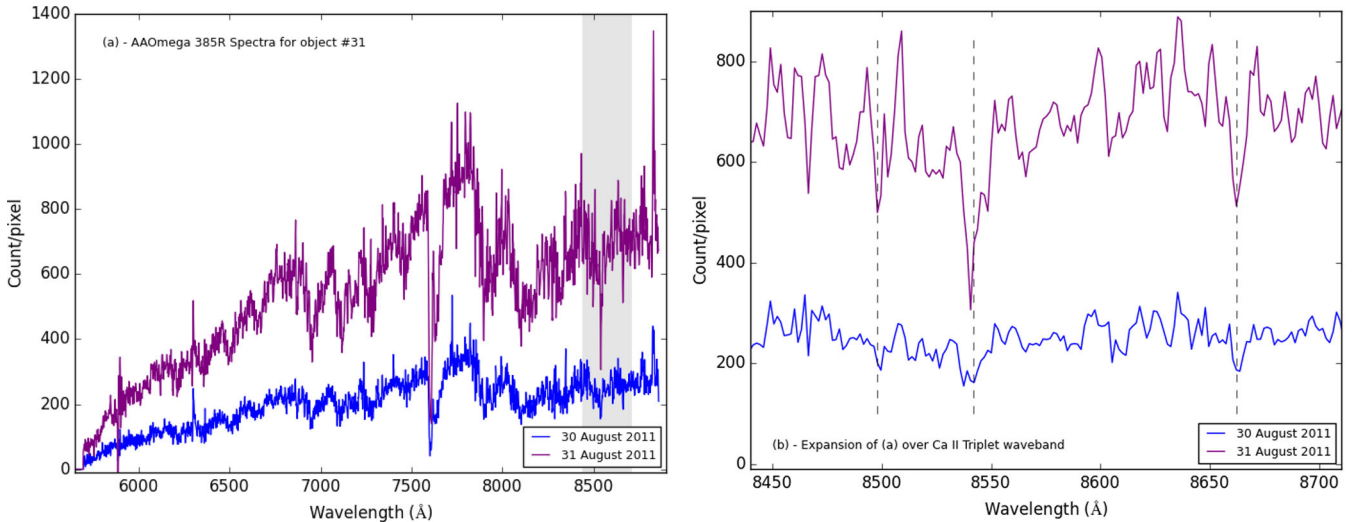
Figure 2. Spectra for object #31. Left-hand panel: full red spectrum from AAOmega grating 385R for object #31 on 2011 August 30 and 31. Object #31 is spectrally classified as a C-type star in Sibbons et al. (2015) and has CN absorption bands at 5730, 6206, 6332, 6478, 6631, 6925, 7088, 7259, 7437, 7876, 8026 Å which are characteristic of this type of star. The large absorption feature at 7594 Å is due to telluric O_2. The grey band indicates the waveband 8440Å to 8710Å containing the Ca II triplet features. Right-hand panel: the same spectra expanded over the waveband 8440–8710 Å containing the Ca II triplet features used for radial velocity measurement. The centres of the Ca II triplet absorption lines are indicated by the vertical dashed lines at 8498.02, 8542.09, and 8662.14 Å.
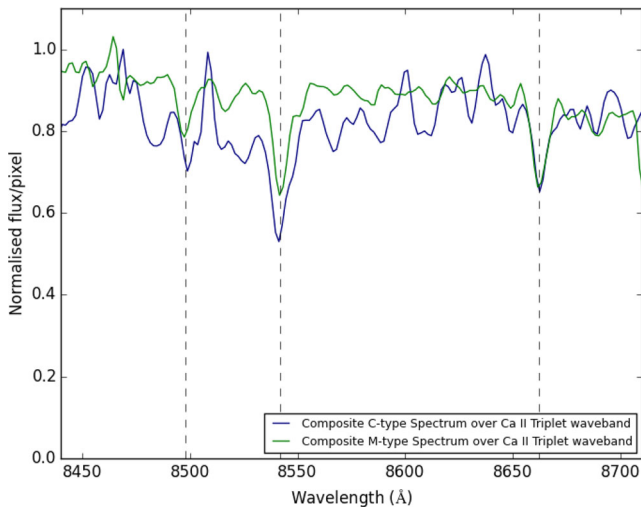

Figure 3. Composite template spectra in the rest frame used for the radial velocity measurements. The centres of Ca II triplet features are shown by the vertical dashed lines.

hght >0.4 yielded velocities within this range so, on this basis, heliocentric velocities falling outside this range were excluded.

4 RESULTS AND ANALYSIS

4.1 Cross-correlation results with the C-type template

All 323 objects were cross-correlated with the C-type composite template. Application of the criteria discussed in Section 3 resulted in 128 successful cross-correlations in the inner region and 107 in the outer region on August 30, and 129 in the inner region and 124 in the outer region on August 31. From the population of 96 C-type AGBs in the inner region, 89 gave results meeting the selection criteria on August 30 and 92 on August 31.

The full results of the radial velocity measurements and their individual errors over both nights are shown in full in the appendix to the electronic version of this paper. The first 18 lines of these results are reproduced in Table 1, with explanations of the column contents. Spectra which failed to meet the selection criteria are not included.

Table 2 summarizes the results. Column (3) shows the mean heliocentric radial velocities, $\langle V_{helio} \rangle$, of the sample. For the inner region, this can be considered a good approximation to the heliocentric radial velocity of NGC 6822. The mean individual error in column (4) is large and reflects the low resolution and low SNR of the spectra. $\sigma(V_{helio})$ in column (5), is the velocity dispersion, which is also high, nevertheless, the standard error of the mean (SE) in column (6) is small, 3–8 km s^{-1}, implying that, provided the individual errors are random, the mean and median (column 7) heliocentric radial velocities are well constrained. The mean velocities show reasonable consistency from night to night, with differences similar to the standard error in the mean, SE. The inner region differs by >−24 km s^{-1} from the outer region[7], supporting the suggestion that the objects in the outer region are not part of NGC 6822.

Thus, we conclude that the heliocentric radial velocity of NGC 6822, as based on the sample of the inner C-type AGB population, lies in the median range of −43 ± 4 to −51 ± 3 km s^{-1} (1σ). The data for August 31 are preferred, owing to their better SNR, lower errors and greater number of successful cross-correlations than the data for August 30, and provides $V_{helio} = -51 \pm 3$ km s^{-1} (1σ). This compares favourably with published values described earlier.

Fig. 4 plots V_{helio} of all objects which meet the acceptance criteria, by distance D from the galactic centre, for both nights. It shows a number of differences between the inner and outer populations. The inner objects tend to clump more closely around the median value for the inner region and they are therefore likely to be part of the

---

[7] This supersedes the preliminary data stated in Sibbons et al. (2015) and is the result of more detailed work.

Table 2. Summary of results for spectra with $hght \geq 0.2$ and $|V_{helio}| < 200$ km s^{-1}.

Template object Composite template	No. of objects (2)	$\langle V_{helio} \rangle$ (km s^{-1}) (3)	$\langle V_{err} \rangle$ (km s^{-1}) (4)	$\sigma(V_{helio})$ (km s^{-1}) (5)	SE (km s^{-1}) (6)	Median V_{helio} (km s^{-1}) (7)
2011 August 30						
Inner region (C-template)	128	−45	±42	45	±4	−43
Outer region (C-template)	107	−20	±63	81	±8	−19
Outer region (M-template)	100	−28	±54	60	±6	−22
2011 August 31						
Inner region (C-template)	129	−51	±32	29	±3	−51
Outer region (C-template)	124	−17	±60	66	±6	−9
Outer region (M-template)	133	−18	±49	58	±5	−19
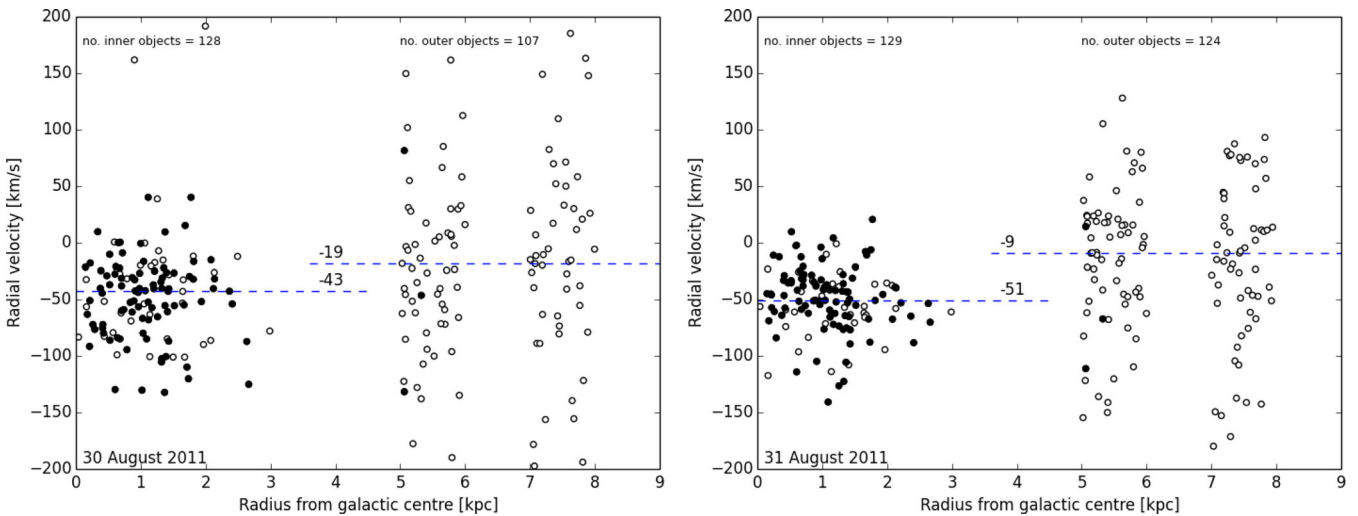
Figure 4. Relationship between V_{helio} and distance D from the galactic centre, left-hand panel for 2011 August 30 and right-hand panel for 2011 August 31. The horizontal dashed lines represent the median radial velocity of the sample from Table 2. C-type AGBs are shown as black points.

same dynamical system, while the outer objects are much more widely spread about a different median value, indicating a separate population. This suggests that the inner population is associated with NGC 6822, supporting similar conclusions in Sibbons et al. (2012, 2015), while the outer population is not.

The aggregated results of the cross-correlation of the spectra of objects in the outer region using the M-type template are also presented in Table 2. Both the formal errors, $\langle V_{err} \rangle$, and the spread of results, $\sigma(V_{helio})$, are reduced by switching to the M-type template in the outer region. The improvement observed in outer region errors when an M-star template is used supports the conclusion that the outer stars are predominantly dM-type, dK-type and other unclassified foreground stars of the Milky Way, (Sibbons et al. 2015).

4.2 Rotation of the carbon star population

In the inner region, the V_{helio} of each C-type object was compared to the sample mean, $\langle V_{helio} \rangle$, which we take to be the mean motion of the galaxy. This provides a measure of the motion of each object in the rest frame of the galactic centre of NGC 6822. Fig. 5 plots the locations of the inner C-stars, colour coded by the value of its residual velocity, $V_{helio} - \langle V_{helio} \rangle$, using a colour range from red (for positive values) to blue (for negative values). The colour range is consistent with red and blue shift and indicates whether an object is

receding or approaching in the rest frame of NGC 6822. In the lower panel for August 31, it can be seen that receding objects dominate the south-east sector and approaching objects the north-west sector, suggesting rotation of the C-star population about an axis, oriented approximately NE-SW. In the upper panel, for the night of August 30, the pattern is less obvious but still apparent.

To examine this further, an axis of rotation was hypothesized lying in the plane of the sky and passing through a pivot point at the centre of the galaxy. The axis was rotated through 360 steps of 1°, starting at a PA of 0°. At each step, the mean of the residual velocities of the stars on either side of the axis was computed. The subsample of stars falling on one side of the line is termed the 'North Bin', and for an axis with PA = 90°, this is defined naturally. The subsample falling on the other side of the line is termed the 'South Bin'. Membership of each bin changes as the axis of rotation sweeps around and the value of its mean velocity residual also changes. By plotting the mean velocity residuals over 360°, a clear rotational signature is observed, see Fig. 6. The purple curves plot the mean rotational velocity of the 'North Bin' and the blue curves plot the mean rotational velocity of the 'South Bin'. In both bins and on both nights the curves rise and fall in opposition as the putative axis is rotated, confirming our impression of a rotating population. Furthermore, the curves for August 30 and 31 both suggest a similar sense of speed and rotation, even though the curves for August 30 are noisier.
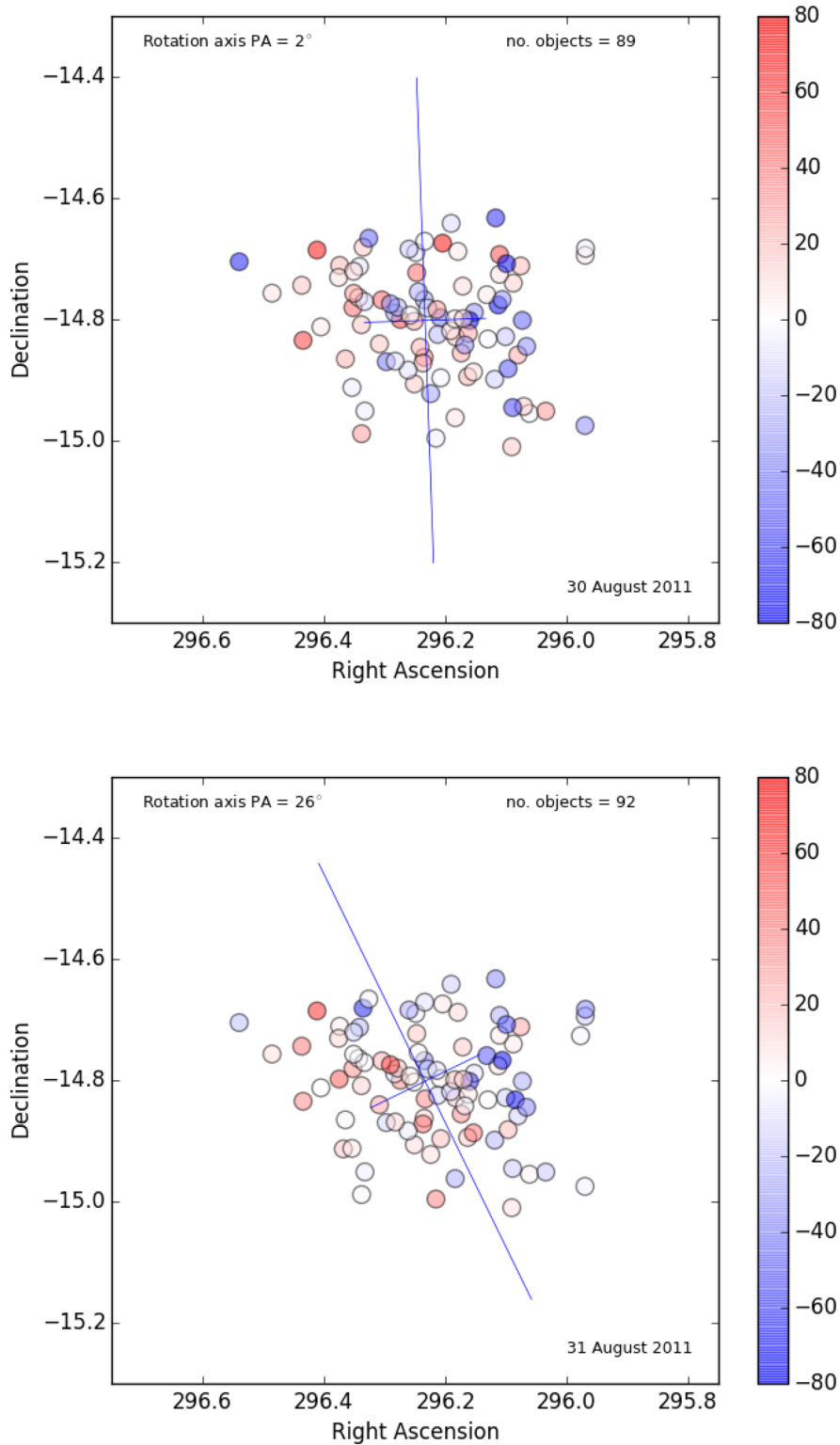
Figure 5. Residual velocity, $V_{helio} - \langle V_{helio} \rangle$, plots of the carbon star sample in the inner region of NGC 6822. The long axis represents a derived axis of rotation and passes through the galaxy centre at the intersection with the short axis.

The green curve in each case shows the sum of the average 'north' and 'south' velocities, which is generally offset from zero as the number of stars in the 'north' and 'south' bins is not always equal at each step. Over the full 360°, the offset should average to zero if the centre of the stellar sample and the pivot point of the hypothesized axis of rotation (the galaxy centre) are coincident. In this case, the green curve appears to lie mainly above the zero line, which suggests that the pivot point adopted does not coincide perfectly with the rotational centre of the sample. Changing the co-ordinates of the galactic centre in our analysis to the centre of
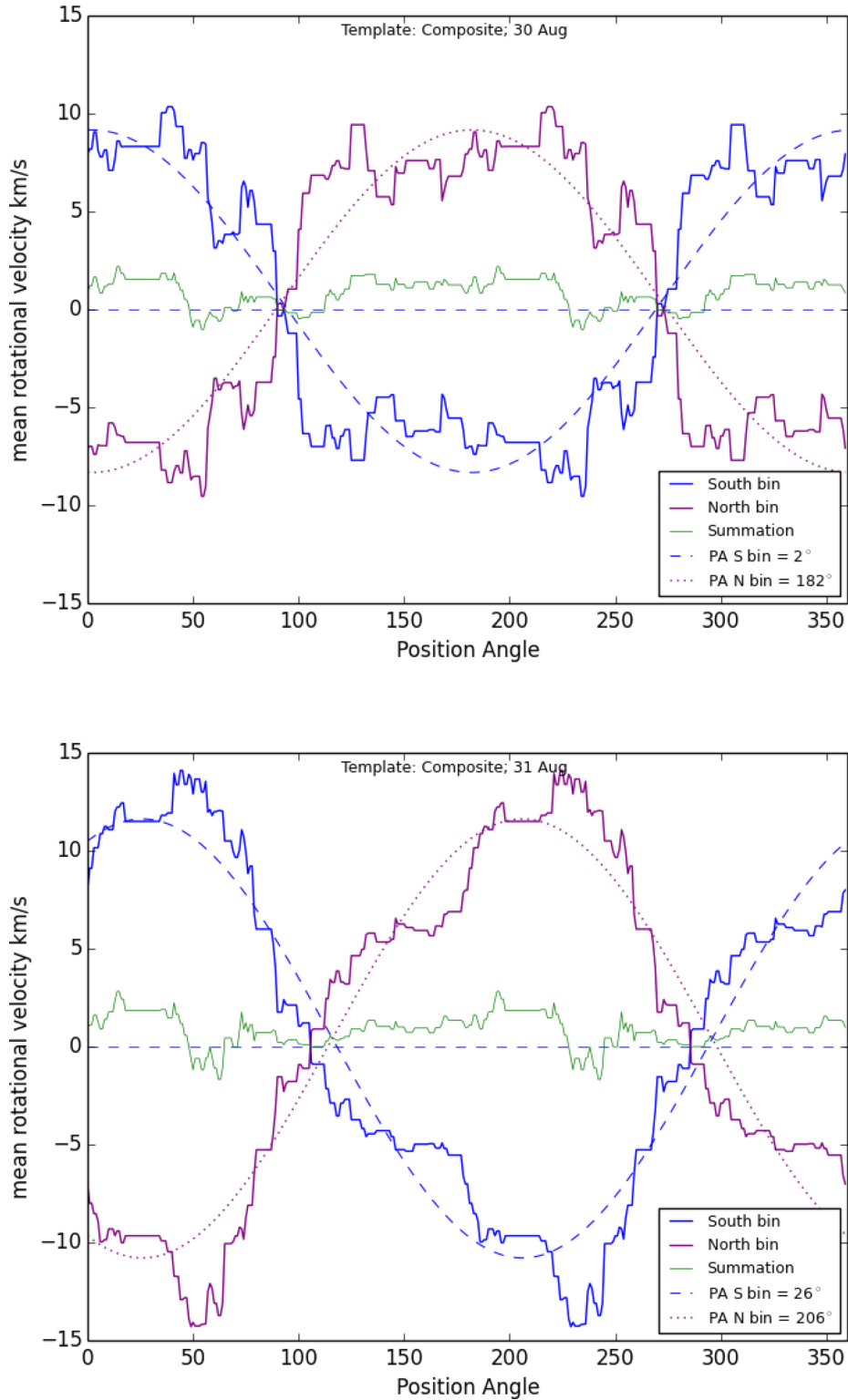
Figure 6. Rotational signature of carbon star component in NGC 6822 derived by plotting the mean residual velocities, $\langle V_{helio} - \langle V_{helio} \rangle \rangle$, on either side of the long axis as a function of its position angle.

the sample eliminates the offset, but has no significant effect on the rotation characteristics.

Using a least-squares method, a sinusoid of the form $\hat{y} = V_{rot} \sin(\theta - \theta_0) + y_0$ was fitted to the measured residual velocities, y, for each bin, such that $(\hat{y} - y)^2$ is minimized. The peak ampli-

tude gives the mean rotational velocity, V_{rot}, θ tracks the PA of the hypothesized axis and is stepped in $1°$ intervals, and θ_0 is the value of θ when $\hat{y} - y_0 = 0$. y_0 is the offset. Solving for y_0, θ_0 and V_{rot}, $\hat{y}$ is plotted in Fig. 6, as dotted and dashed sinusoids for the 'north' and 'south' bins, respectively. The rotation axis PA occurs at the

Table 3. Summary of sinusoidal least-squares fit to mean residual velocities.

	Rotation rate		Rotation axis		Offset
	V_{rot} km s^{-1} (1)	ΔV_{rot} km s^{-1} (2)	PA $^{\circ}$ (3)	ΔPA $^{\circ}$ (4)	y_0 km s^{-1} (5)
2011 Aug 30	8.7	±2.2	2°	±22°	0.4
2011 Aug 31	11.2	±2.1	26°	±13°	0.4

peak of the sinusoid, so its PA is given by the value of θ when $\hat{y}$ is a maximum. This occurs at $\theta_0 \pm 90°$.

Table 3 provides a summary of the results obtained, with V_{rot} in column (1). In column (2), we calculate the error in the velocity amplitude, ΔV_{rot}, from the RMS of the residual velocities found by deducting the sine function from each measured value over 360°, at the best-fitting PA. In columns (3) and (4), we show the PA of the galactic rotation axis and an estimate of its positional error found by taking the RMS, over 360°, of $\theta - \theta'$, where θ' is the angle which gives the value of $\hat{y}(\theta)$ in the sine function at the best-fitting PA. Column (5) shows the mean offset of the sinusoid due to the axis pivot point and the sample centre not being coincident.

The sense of rotation on both nights is the same and is such that the southeastern side is receding and the northwestern side is approaching, which corresponds with the rotation of H I gas in Weldrake et al. (2003). Moreover the rotation velocities and estimated PA for each night correspond within the estimated errors which gives us good confidence in the result. Nevertheless, owing to the better quality spectra for August 31, better SNR and better error results, we take the results for August 31, i.e. $V_{rot} = 11.4 \pm 2.1$ km s^{-1} and PA = 26 ± 13° as the more reliable.

Up to now, we have been considering only objects <4 kpc from the galaxy centre. These correspond to objects in the Letarte et al. (2002) catalogue. Nevertheless there are three outliers at distances ∼5 kpc, which lie close to the stellar ellipse in Fig. 1 and which are classified as C-type AGBs (Sibbons et al. 2015). These objects lie in positions close to the major axis of the ellipse. If we include these outliers in our estimates, the rotation rate and rotation axis become $V_{rot} = 11.2 \pm 2.5$ km s^{-1} $PA = -5° \pm 20°$ for August 30 and $V_{rot} = 12.1 \pm 2.3$ km s^{-1} PA = 19° ± 14° for August 31, well within the margins of error for our sample.

5 DISCUSSION AND CONCLUSION

Table 4 compares our results with the published data previously summarized in Section 1. The heliocentric radial velocity we obtained for NGC 6822 is -51 ± 3 km s^{-1}, based on the results from the better of the two nights of observations of a sample of its intermediate age carbon star population. This is a little lower than its H I counterpart – -57 ± 2 km s^{-1} – (Koribalski et al. 2004) but shows less than 1.6σ difference to this and the other estimates above, except that of Hwang et al. (2014) where it is apparent that the errors in Hwang et al. (2014) are large enough to include our result. In our sample, the grouping of objects in the inner and outer regions of the observed field indicates that the inner objects belong to NGC 6822, while the outer objects are more likely to be Milky Way stars, in support of the conclusion in Sibbons et al. (2015).

Rotation of the carbon star population about an axis having PA = 26 ± 13° has been shown with a rotation speed $V_{rot} = 11.2 \pm 2.1$ km s^{-1}, based on the better of the two observing nights. While we see some movement in the PA of the rotation axis due to the AGB outliers in Fig. 1, their numbers are too small to draw any real conclusions on its significance. Radial velocity data from more objects spread broadly throughout the stellar ellipse in Fig. 1 would provide better data. Nevertheless, the sense of rotation of the sample is that the SE corner is receding and the NW corner is approaching, similar to the rotation of the H I disc (Weldrake et al. 2003). We can infer from Weldrake et al. (2003), that the PA of the rotation axis of the H I disc is ∼20° to ∼40° in the plane of the sky, assuming the rotation axis is perpendicular to the major axis of the gas disc. This is comparable to our estimate of the sky projected rotation axis of the C-type stellar population in this study. Thus we find that both axes are approximately coincident and the sense of rotation of the stars and gas is the same, leading us to conclude that NGC 6822 is not a PRG.

The PA of the major axes of the isodensity contours of the RGB stars in Demers et al. (2006) varies from 80° for the innermost contour (radius =10 arcmin) to 65° for the outermost contour (radius = 35 arcmin). Our inner sample has an angular radius of ∼17 arcmin, and so falls between these extremes. Hence, there is a misalignment of ∼45° between our rotation axis and the respective isodensity profile. Furthermore, since V_{rot} is derived from mean velocities, it is reasonable to adopt the mean distance of our carbon star sample from the galaxy centre as a basis for further comparative discussion. This distance is $\langle D \rangle = 1.1$ kpc. Interpreting the velocity diagrams of Weldrake et al. (2003), the rotation speed of the H I disc

Table 4. Comparison of results with published velocity data.

		V_{helio} (km s^{-1})	V_{rot} (km s^{-1})	Rotation axis PA	Comments
This study		-51 ± 3	11.2 ± 2.1	26° ± 13°	92 carbon stars
Koribalski et al. (2004)	[1]	-57 ± 2	–	–	H I measurements
Weldrake et al. (2003)	[2]	-53.3 to -54.7	-100 to $+10$	–	H I measurements
McConnachie (2012)		-57 ± 2.0	47 ± 2	–	V_{helio} from [1]
Mateo (1998)		–	47 ± 3	–	H I measurements
Mateo (1998)		-53 ± 4	–	–	Optical measurements
Kirby et al. (2014)		-54 ± 1.7	∼10	–	292 red giant stars
Demers et al. (2006)	[3]	$+10$ to -70	–	63° to 67°	110 carbon stars
Veljanoski et al. (2015)		-59 to -60	12 ± 10	–	8 GCs, 'disc' model, see Section 1
Flores-Durán et al. (2014)		-57.8	–	–	10 Planetary nebulae
Hwang et al. (2014)		-88.3 ± 22.7	–.	–	4 Extended star clusters
Hwang et al. (2014)		-32.9 ± 29.4	15.9 ± 0.3	–	Derived from carbon star population of [3]

can be estimated to be ∼30 km s^{-1} at 1.1 kpc (≈8 arcmin) from the galactic centre. This rotation speed is faster than our C-star sample confirming differences in the rotation speeds of the rotationally supported gas and the pressure supported intermediate age stellar populations.

The rotation misalignment, apparent separation of gas and stellar populations and effect of AGBs filling the gap between the central sample in this study and the stellar ellipse depicted in Fig. 1 would benefit from further study, particularly at higher SNR and better resolving power.

ACKNOWLEDGEMENTS

REFERENCES

Battinelli P., Demers S., Kunkel W. E., 2006, A&A, 451, 99
de Blok W. J. G., Walter F., 2000, ApJ, 537, L95
Demers S., Battinelli P., 2007, in Kerschbaum F., Charbonnel C., Wing R. F., eds, ASP Conf. Ser. Vol. 378, Why Galaxies Care About AGB Stars: Their Importance as Actors and Probes. Astron. Soc. Pac., San Francisco, p. 469
Demers S., Battinelli P., Kunkel W. E., 2006, ApJ, 636, L85
Feast M. W., Whitelock P. A., Menzies J. W., Matsunaga N., 2012, MNRAS, 421, 2998
Flores-Durán S. N., Peña M., Hernández-Martínez L., García-Rojas J., Ruiz M. T., 2014, A&A, 568, A82
Gieren W., Pietrzyński G., Nalewajko K., Soszyński I., Bresolin F., Kudritzki R.-P., Minniti D., Romanowsky A., 2006, ApJ, 647, 1056
Hodge P., Smith T., Eskridge P., MacGillivray H., Beard S., 1991, ApJ, 379, 621
Hubble E., 1925, Contrib. Mount Wilson Obs, 304, 1
Hwang N., Park H. S., Lee M. G., Lim S., Hodge P. W., Kim S. C., Miller B., Weisz D., 2014, ApJ, 783, 49
Kirby E. N., Bullock J. S., Boylan-Kolchin M., Kaplinghat M., Cohen J. G., 2014, MNRAS, 439, 1015
Koribalski B. S. et al., 2004, AJ, 128, 16
Letarte B., Demers S., Battinelli P., Kunkel W. E., 2002, AJ, 123, 832
McConnachie A. W., 2012, AJ, 144, 4
Mateo M. L., 1998, ARA&A, 36, 435
Matthews L. D., Gérard E., Le Bertre T., 2015, MNRAS, 449, 220
Rich J. A., Persson S. E., Freedman W. L., Madore B. F., Monson A. J., Scowcroft V., Seibert M., 2014, ApJ, 794, 107
Sibbons L. F., Ryan S. G., Cioni M.-R. L., Irwin M., Napiwotzki R., 2012, A&A, 540, A135
Sibbons L. F., Ryan S. G., Napiwotzki R., Thompson G. P., 2015, A&A, 574, A102
Tonry J., Davis M., 1979, AJ, 84, 1511
van Belle G. T., Paladini C., Aringer B., Hron J., Ciardi D., 2013, ApJ, 775, 45
Veljanoski J. et al., 2015, MNRAS, 452, 320
Weldrake D. T. F., de Blok W. J. G., Walter F., 2003, MNRAS, 340, 12
Whitelock P. A., Menzies J. W., Feast M. W., Nsengiyumva F., Matsunaga N., 2013, MNRAS, 428, 2216

SUPPORTING INFORMATION

Additional Supporting Information may be found in the online version of this article:

Appendix A. Tables of data.
(http://www.mnras.oxfordjournals.org/lookup/suppl/doi: 10.1093/mnras/stw1193/-/DC1).

Please note: Oxford University Press is not responsible for the content or functionality of any supporting materials supplied by the authors. Any queries (other than missing material) should be directed to the corresponding author for the article.

This paper has been typeset from a T$_{\text{E}}$X/L^{A}T$_{\text{E}}$X file prepared by the author.